Title

Cerebral blood flow is decoupled from blood pressure and linked to EEG bursting after resuscitation from cardiac arrest.

Journal

Biomedical Optics Express, 7(11)

ISSN

2156-7085

Authors

Crouzet, Christian
Wilson, Robert H
Bazrafkan, Afsheen
et al.

Publication Date

2016-11-01

DOI

10.1364/boe.7.004660

Peer reviewed

Research Article | Vol. 7, No. 11 | 1 Nov 2016 | BIOMEDICAL OPTICS EXPRESS 4660
Biomedical Optics EXPRESS

Cerebral blood flow is decoupled from blood pressure and linked to EEG bursting after resuscitation from cardiac arrest

CHRISTIAN CROUZET,[1,2] ROBERT H. WILSON,[1] AFSHEEN BAZRAFKAN,[3] MARYAM H. FARAHABADI,[3,4] DONALD LEE,[3] JUAN ALCOCER,[3] BRUCE J. TROMBERG,[1,2,5] BERNARD CHOI,[1,2,5,6] AND YAMA AKBARI[3,4,*]

[1]*Beckman Laser Institute and Medical Clinic, University of California, Irvine, CA 92617, USA*
[2]*Department of Biomedical Engineering, University of California, Irvine, CA 92697, USA*
[3]*Department of Neurology, University of California, Irvine, CA 92697, USA*
[4]*School of Medicine, University of California, Irvine, CA 92697, USA*
[5]*Department of Surgery, University of California, Irvine, CA 92868, USA*
[6]*Edwards Lifesciences Center for Advanced Cardiovascular Technology, University of California, Irvine, CA 92697, USA*
**yakbari@uci.edu*

Abstract: In the present study, we have developed a multi-modal instrument that combines laser speckle imaging, arterial blood pressure, and electroencephalography (EEG) to quantitatively assess cerebral blood flow (CBF), mean arterial pressure (MAP), and brain electrophysiology before, during, and after asphyxial cardiac arrest (CA) and resuscitation. Using the acquired data, we quantified the time and magnitude of the CBF hyperemic peak and stabilized hypoperfusion after resuscitation. Furthermore, we assessed the correlation between CBF and MAP before and after stabilized hypoperfusion. Finally, we examined when brain electrical activity resumes after resuscitation from CA with relation to CBF and MAP, and developed an empirical predictive model to predict when brain electrical activity resumes after resuscitation from CA. Our results show that: 1) more severe CA results in longer time to stabilized cerebral hypoperfusion; 2) CBF and MAP are coupled before stabilized hypoperfusion and uncoupled after stabilized hypoperfusion; 3) EEG activity (bursting) resumes after the CBF hyperemic phase and before stabilized hypoperfusion; 4) CBF predicts when EEG activity resumes for 5-min asphyxial CA, but is a poor predictor for 7-min asphyxial CA. Together, these novel findings highlight the importance of using multi-modal approaches to investigate CA recovery to better understand physiological processes and ultimately improve neurological outcome.

OCIS codes: (110.6150) Speckle imaging; (120.5475) Pressure measurement; (170.2655) Functional monitoring and imaging; (170.3880) Medical and biological imaging; (170.5380) Physiology; (170.1610) Clinical applications.

References and links

1. D. Mozaffarian, E. J. Benjamin, A. S. Go, D. K. Arnett, M. J. Blaha, M. Cushman, S. De Ferranti, J. P. Després, H. J. Fullerton, V. J. Howard, M. D. Huffman, S. E. Judd, B. M. Kissela, D. T. Lackland, J. H. Lichtman, L. D. Lisabeth, S. Liu, R. H. Mackey, D. B. Matchar, D. K. McGuire, E. R. Mohler, C. S. Moy, P. Muntner, M. E. Mussolino, K. Nasir, R. W. Neumar, G. Nichol, L. Palaniappan, D. K. Pandey, M. J. Reeves, C. J. Rodriguez, P. D. Sorlie, J. Stein, A. Towfighi, T. N. Turan, S. S. Virani, J. Z. Willey, D. Woo, R. W. Yeh, and M. B. Turner, *Heart Disease and Stroke Statistics-2015 Update : A Report from the American Heart Association* (2015), Vol. 131.
2. A. Schneider, B. W. Böttiger, and E. Popp, "Cerebral resuscitation after cardiocirculatory arrest," Anesth. Analg. **108**(3), 971–979 (2009).
3. S. Laver, C. Farrow, D. Turner, and J. Nolan, "Mode of death after admission to an intensive care unit following cardiac arrest," Intensive Care Med. **30**(11), 2126–2128 (2004).
4. J. K. Lee, K. M. Brady, J. O. Mytar, K. K. Kibler, E. L. Carter, K. G. Hirsch, C. W. Hogue, R. B. Easley, L. C. Jordan, P. Smielewski, M. Czosnyka, D. H. Shaffner, and R. C. Koehler, "Cerebral blood flow and cerebrovascular autoregulation in a swine model of pediatric cardiac arrest and hypothermia," Crit. Care Med. **39**(10), 2337–2345 (2011).

#270564 http://dx.doi.org/10.1364/BOE.7.004660
Journal © 2016 Received 18 Jul 2016; revised 5 Oct 2016; accepted 10 Oct 2016; published 20 Oct 2016

Biomedical Optics EXPRESS

5. C. Sundgreen, F. S. Larsen, T. M. Herzog, G. M. Knudsen, S. Boesgaard, and J. Aldershvile, "Autoregulation of cerebral blood flow in patients resuscitated from cardiac arrest," Stroke **32**(1), 128–132 (2001).
6. L. L. Bisschops, C. W. Hoedemaekers, K. S. Simons, and J. G. van der Hoeven, "Preserved metabolic coupling and cerebrovascular reactivity during mild hypothermia after cardiac arrest," Crit. Care Med. **38**(7), 1542–1547 (2010).
7. E. Mörtberg, P. Cumming, L. Wiklund, A. Wall, and S. Rubertsson, "A PET study of regional cerebral blood flow after experimental cardiopulmonary resuscitation," Resuscitation **75**(1), 98–104 (2007).
8. E. Edgren, P. Enblad, A. Grenvik, A. Lilja, S. Valind, L. Wiklund, U. Hedstrand, H. Stjernström, L. Persson, U. Pontén, and B. Långström, "Cerebral blood flow and metabolism after cardiopulmonary resuscitation. A pathophysiologic and prognostic positron emission tomography pilot study," Resuscitation **57**(2), 161–170 (2003).
9. M. D. Manole, L. M. Foley, T. K. Hitchens, P. M. Kochanek, R. W. Hickey, H. Bayir, H. Alexander, C. Ho, and R. S. B. Clark, "Magnetic resonance imaging assessment of regional cerebral blood flow after asphyxial cardiac arrest in immature rats," J. Cereb. Blood Flow Metab. **29**(1), 197–205 (2009).
10. T. Drabek, L. M. Foley, A. Janata, J. Stezoski, T. K. Hitchens, M. D. Manole, and P. M. Kochanek, "Global and regional differences in cerebral blood flow after asphyxial versus ventricular fibrillation cardiac arrest in rats using ASL-MRI," Resuscitation **85**(7), 964–971 (2014).
11. X. Jia, M. A. Koenig, A. Venkatraman, N. V. Thakor, and R. G. Geocadin, "Post-cardiac arrest temperature manipulation alters early EEG bursting in rats," Resuscitation **78**(3), 367–373 (2008).
12. X. Jia, M. A. Koenig, H. C. Shin, G. Zhen, C. A. Pardo, D. F. Hanley, N. V. Thakor, and R. G. Geocadin, "Improving neurological outcomes post-cardiac arrest in a rat model: immediate hypothermia and quantitative EEG monitoring," Resuscitation **76**(3), 431–442 (2008).
13. M. C. Cloostermans, F. B. van Meulen, C. J. Eertman, H. W. Hom, and M. J. van Putten, "Continuous electroencephalography monitoring for early prediction of neurological outcome in postanoxic patients after cardiac arrest: a prospective cohort study," Crit. Care Med. **40**(10), 2867–2875 (2012).
14. H. Søholm, T. W. Kjær, J. Kjaergaard, T. Cronberg, J. Bro-Jeppesen, F. K. Lippert, L. Køber, M. Wanscher, and C. Hassager, "Prognostic value of electroencephalography (EEG) after out-of-hospital cardiac arrest in successfully resuscitated patients used in daily clinical practice," Resuscitation **85**(11), 1580–1585 (2014).
15. G. Buunk, J. G. van der Hoeven, and A. E. Meinders, "Cerebral blood flow after cardiac arrest," Neth. J. Med. **57**(3), 106–112 (2000).
16. C. S. Robertson, "Management of cerebral perfusion pressure after traumatic brain injury," Anesthesiology **95**(6), 1513–1517 (2001).
17. Junyun He, Hongyang Lu, Ruoxian Deng, L. Young, Shanbao Tong, and Xiaofeng Jia, "Real-time monitoring of cerebral blood flow by laser speckle contrast imaging after cardiac arrest in rat," Conf. Proc. IEEE Eng. Med. Biol. Soc. **2015**, 6971–6974 (2015).
18. M. Oddo and A. O. Rossetti, "Predicting neurological outcome after cardiac arrest," Curr. Opin. Crit. Care **17**(3), 254–259 (2011).
19. J. C. Ramirez-San-Juan, R. Ramos-García, I. Guizar-Iturbide, G. Martínez-Niconoff, and B. Choi, "Impact of velocity distribution assumption on simplified laser speckle imaging equation," Opt. Express **16**(5), 3197–3203 (2008).
20. N. Bruder, D. Pellissier, P. Grillot, and F. Gouin, "Cerebral hyperemia during recovery from general anesthesia in neurosurgical patients," Anesth. Analg. **94**, 650–654 (2002).
21. X. Y. Yang, S. J. Zhou, Y. F. Yu, Y. F. Shen, and H. Z. Xu, "Cerebral hyperaemia after isoflurane anaesthesia for craniotomy of patients with supratentorial brain tumour," Acta Anaesthesiol. Scand. **57**(10), 1301–1307 (2013).
22. K. A. Ludwig, R. M. Miriani, N. B. Langhals, M. D. Joseph, D. J. Anderson, and D. R. Kipke, "Using a common average reference to improve cortical neuron recordings from microelectrode arrays," J. Neurophysiol. **101**(3), 1679–1689 (2009).
23. Y. Xu, S. Liachenko, and P. Tang, "Dependence of early cerebral reperfusion and long-term outcome on resuscitation efficiency after cardiac arrest in rats," Stroke **33**(3), 837–843 (2002).
24. J. S. B. Shaik, S. M. Poloyac, P. M. Kochanek, H. Alexander, D. L. Tudorascu, R. S. Clark, and M. D. Manole, "20-Hydroxyeicosatetraenoic Acid Inhibition by HET0016 Offers Neuroprotection, Decreases Edema, and Increases Cortical Cerebral Blood Flow in a Pediatric Asphyxial Cardiac Arrest Model in Rats," J. Cereb. Blood Flow Metab. **35**(11), 1757–1763 (2015).
25. J. Hofmeijer, M. C. Tjepkema-Cloostermans, and M. J. A. M. van Putten, "Burst-suppression with identical bursts: a distinct EEG pattern with poor outcome in postanoxic coma," Clin. Neurophysiol. **125**(5), 947–954 (2014).
26. E. Westhall, I. Rosén, A. O. Rossetti, A.-F. van Rootselaar, T. W. Kjaer, J. Horn, S. Ullén, H. Friberg, N. Nielsen, and T. Cronberg, "Electroencephalography (EEG) for neurological prognostication after cardiac arrest and targeted temperature management; rationale and study design," BMC Neurol. **14**(1), 159 (2014).
27. B. Chen, F. Q. Song, L. L. Sun, L. Y. Lei, W. N. Gan, M. H. Chen, and Y. Li, "Improved early postresuscitation EEG activity for animals treated with hypothermia predicted 96 hr neurological outcome and survival in a rat model of cardiac arrest," BioMed Res. Int. **2013**, 312137 (2013).
28. K. P. Nadeau, T. B. Rice, A. J. Durkin, and B. J. Tromberg, "Multifrequency synthesis and extraction using square wave projection patterns for quantitative tissue imaging," J. Biomed. Opt. **20**(11), 116005 (2015).

Biomedical Optics EXPRESS

29. A. K. Dunn, A. Devor, H. Bolay, M. L. Andermann, M. A. Moskowitz, A. M. Dale, and D. A. Boas, "Simultaneous imaging of total cerebral hemoglobin concentration, oxygenation, and blood flow during functional activation," Opt. Lett. **28**(1), 28–30 (2003).
30. A. K. Dunn, A. Devor, A. M. Dale, and D. A. Boas, "Spatial extent of oxygen metabolism and hemodynamic changes during functional activation of the rat somatosensory cortex," Neuroimage **27**(2), 279–290 (2005).

1. Introduction

According to the American Heart Association, over 500,000 Americans suffer a cardiac arrest (CA) per year [1]. Although resuscitation efforts have improved [2], poor neurological outcome is the leading cause of morbidity in CA survivors, and only 8.3% of out-of-hospital CA survivors have good neurological recovery [1,3]. To improve neurological outcome and understand how the brain recovers following CA, a critical need exists to investigate physiological processes that impact the brain, such as cerebral blood flow (CBF), arterial blood pressure, and brain electrophysiology.

Many clinical and preclinical studies have investigated the dynamics of brain physiology.These studies have used a multitude of techniques to examine cerebral blood flow and electrophysiology following CA, such as Doppler techniques [4–6], positron emission tomography (PET) [7,8], magnetic resonance imaging (MRI) [9,10], and electroencephalography (EEG) [11–14]. CBF studies have reported a hyperemic phase, followed by a stabilized hypoperfusion phase, before CBF steadily increases toward baseline over 24h [15]. A common metric clinicians use to determine if the brain receives an adequate amount of CBF is cerebral perfusion pressure (CPP) [16]. CPP is defined as the difference between mean arterial pressure (MAP) and intracranial pressure (ICP), which represents the pressure gradient that drives CBF.Studies have examined the impact that CBF autoregulation has on patient outcome [5], and the dysregulation of CBF from MAP after return of spontaneous circulation (ROSC) or resuscitation [17]. EEG studies have found that an isoelectric period occurs immediately after resuscitation, until bursting (defined as a sharp increase in EEG amplitude interspersed between isoelectric periods) begins.Furthermore, continuous brain electrical activity 24h post-ROSC is associated with improved neurological outcome [18]. Although these studies have vastly expanded our understanding of brain functional dynamics following CA, they have two main shortcomings: 1) hemodynamic techniques have poor temporal resolution (~5–30min); and 2) lack of simultaneous multi-modal approaches to relate CBF, MAP, and brain electrophysiology.

To address these shortcomings, we developed a multi-modal instrument design that combines laser speckle imaging (LSI), arterial blood pressure, and EEG to simultaneously acquire data before, during, and after CA and resuscitation. Due to the relatively high temporal resolution (~seconds) of our instrument, our results quantify the time and magnitude of the hyperemic peak and stabilized hypoperfusion post-ROSC. Furthermore, we assess the correlation between CBF and MAP before and after stabilized hypoperfusion. Finally, we show that initial EEG bursting begins after the CBF hyperemic phase and before stabilized hypoperfusion, and we can accurately predict when the initial EEG burst occurs for less severe CA. Collectively, our findings indicate the importance of using multi-modal approaches to better understand the physiological processes of CA recovery and ultimately improve neurological outcome.

2. Materials and methods

2.1 Animal model

We performed experiments on 16 male Wistar rats (351 ± 39g in mass). The asphyxial CA model and study protocol (no. 2013-3098) were approved in accordance with the Institutional Animal Care and Use Committee at University of California, Irvine. After applying the inclusion criterion that chest compressions lasted shorter than 1min, the final number of rats included for data analysis was 13 (n = 7, 5-min asphyxia; and n = 6, 7-min asphyxia).

Biomedical Optics EXPRESS

2.2 Animal preparation and surgery

We developed an asphyxial CA model similar to those used in previous studies [9,11]. Rats were calorically restricted the night prior to CA experiments. On the day of CA, rats were anesthetized and intubated using a 14-gauge endotracheal tube (B. Braun Melsungen AG, Melsungen, Germany), which was connected to a TOPO mechanical ventilator (Kent Scientific, Torrington, CT) and isoflurane vaporizer. During surgery, isoflurane was maintained at 2% and ventilation settings were maintained at 70 breaths per min (BPM), with 12–14cmH_2O peak inspiration pressure (PIP) and 3cmH_2O peak end expiratory pressure (PEEP) in a 50%/50% N_2/O_2 mixture at 2LPM. Rectal temperature (Kent Scientific, Torrington, CT) was continuously measured and maintained between 36.5 and 37.5°C. The rat was then mounted onto a stereotaxic frame (Kopf Instruments, Tujunga, CA) to stabilize the head position for surgery.

A midline incision was performed over the scalp and the scalp retracted to expose the skull for EEG electrode implantation (Plastics One Inc., Roanoke, VA). Two frontal electrodes were implanted (2mm anterior and 2.5mm lateral to bregma), and one electrode was implanted over the visual cortex (5.5mm posterior to bregma and 4mm left of bregma). A reference electrode was placed 3mm posterior to lambda. Following the implantation of EEG electrodes, a 4mm x 6mm craniectomy was performed over the right sensory and visual cortex using a power micro-drill (Roboz Surgical Instrument Co., Gaithsburg, Maryland) to enable subsequent optical imaging. Saline was applied periodically to ensure the brain stayed hydrated. Following the craniectomy, the femoral artery and vein were cannulated using PE-50 tubing (Becton, Dickinson and Company, Franklin Lakes, NJ). Invasive arterial blood pressure was measured continuously using a transducer (CWE Inc., Ardmore, PA). Baseline arterial blood gas (ABG) measurements (Abaxis, Union City, CA) were obtained within 30min prior to initiation of asphyxia.

2.3 Asphyxial cardiac arrest and resuscitation

A timeline of the CA experiments is depicted in Fig. 1(A). At experiment start time, rats were placed on 100% O_2, while isoflurane was reduced to 0.5–1% to prepare for anesthesia wash out. At 2min into the experiment, room air (21% O_2) was given, isoflurane was turned off to wash out anesthesia, and neuromuscular blockade initiated with 1mL of intravenous Vecuronium (2mg/kg), flushed with 1mL of heparinized saline. At 5min, asphyxia was initiated by turning the ventilator off and tubing clamped. Rats were subjected to a period of either 5- or 7-min asphyxia. CA was defined as a systolic blood pressure <30mmHg and pulse pressure <10mmHg. Thirty seconds prior to chest compressions, mechanical ventilation was re-initiated at 100% O_2 with respiratory rate of 75–85BPM, PIP of 17.5–18.5 cmH_2O, and PEEP of 3cmH_2O at 2.5LPM. Epinephrine (0.01mg/kg) and sodium bicarbonate (1mmol/kg) were administered intravenously, followed by 2mL of heparinized saline prior to initiation of chest compressions. Chest compressions continued until return of spontaneous circulation (ROSC). ABGs were obtained 10-min post-ROSC and 40 min thereafter, to assess ventilation and modify ventilator settings as necessary.

Biomedical Optics EXPRESS

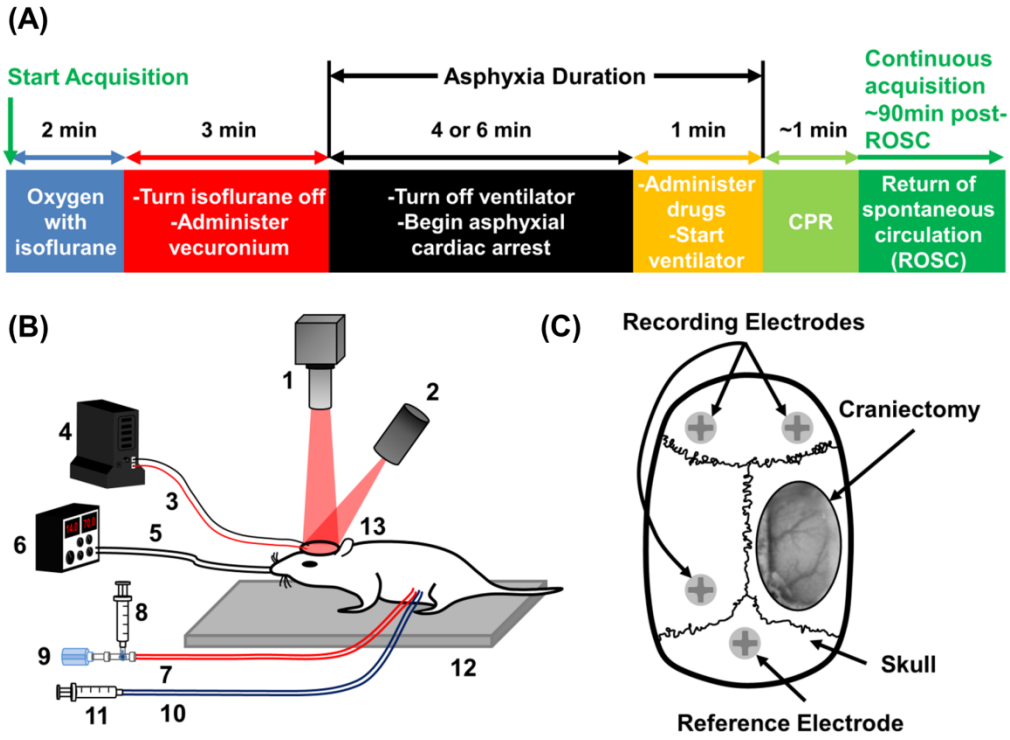

Fig. 1. Cardiac arrest (CA) experimental design and setup. (A) Diagram of CA timeline. Experiment began (t = 0) with an isoflurane/oxygen mix. At t = 2min, isoflurane was turned off, Vecuronium administered, and animal exposed to room air. The ventilator was then turned off to initiate the asphyxial CA period that lasted 5- or 7-min. Approximately 1min prior to initiation of cardiopulmonary resuscitation (CPR), epinephrine, sodium bicarbonate and saline were administered and the ventilator restarted. CPR was then performed for ~1min until ROSC, after which data acquisition continued for ~90min post-ROSC. (B) Schematic of multi-instrument design to perform laser speckle imaging (LSI), arterial blood pressure measurements, and electroencephalography (EEG). (1) LSI camera with laser line filter and adjustable camera lens; (2) 809nm light source for LSI to display speckle pattern on rat cortex; (3) EEG wire that connected EEG screw electrodes to EEG preamplifier; (4) EEG preamplifier with 0.35Hz high pass filter; (5) intubation tubing connected to ventilator; (6) ventilator with adjustable settings; (7) femoral artery catheter; (8) syringe to administer fluids for dehydration and remove blood for arterial blood gas (ABG) measurements; (9) blood pressure transducer; (10) femoral vein catheter; (11) syringe to administer epinephrine, sodium bicarbonate and saline prior to CPR and ROSC; (12) stereotaxic frame with rat mounted; (13) brain illuminated by laser light with EEG screw electrodes. (C) Magnified view of animal head that shows location of EEG electrodes and craniectomy.

2.4 Multi-modal instrument design and data acquisition

To accomplish our multi-modal approach of monitoring CBF, arterial blood pressure, and brain electrophysiology before, during, and after CA and resuscitation, we combined LSI, arterial blood pressure, and EEG, as shown in Fig. 1(B). All technologies were simultaneously recorded throughout the entire experiment.

To measure CBF, LSI was used. As an excitation source we used a stabilized 809nm laser (Ondax, Monrovia, CA) with a long coherence length. The laser was sent through expansion optics and a ground glass diffuser (ThorLabs, Inc., Newton, NJ) to achieve near-uniform illumination over the craniectomy region (Fig. 1(C)). The remitted light was sent through a laser line filter and raw speckle images were sampled at ~10fps using a Point Grey camera (Point Grey Research Inc., Richmond, BC, Canada) with a 10ms exposure time.

Biomedical Optics EXPRESS

To measure arterial blood pressure, systolic and diastolic blood pressures were recorded from the femoral artery (Fig. 1(B)) at 1Hz. MAP was calculated from the extracted systolic and diastolic blood pressures.

To perform EEG, screw electrodes were used (Fig. 1(C)). EEG data acquisition was recorded from each implanted electrode at 1526Hz with a PZ2 preamplifier (Tucker-Davis Technologies Inc., Alachua, FL) equipped with a first-order high-pass filter (0.35Hz). Acquired data were extracted and further filtering and analysis performed as described in the next section.

2.5 Data processing and statistical analysis

LSI processing used custom-written MATLAB code to process each raw speckle image and obtain CBF information. We used a sliding 5 x 5 square structuring element to convert each raw speckle image to a corresponding speckle contrast image. Equation (1) was performed at each location of the structuring element:

$$K = \frac{\sigma}{< I >} \tag{1}$$

We then converted each speckle contrast image to a speckle flow index (SFI) map using a simplified speckle imaging equation [19]:

$$SFI = \frac{1}{2TK^2} \tag{2}$$

where K is the speckle contrast and T is the exposure time of the camera in seconds. A representative region of interest (ROI) was then selected within the craniectomy to obtain an average SFI value and create time-resolved CBF curves. We then calculated relative SFI curves Eq. (3), and applied a sliding median filter of 10s in length.

$$relative\ SFI = 100 \times \frac{SFI(t)}{baseline\ SFI} \tag{3}$$

Baseline was defined as the mean SFI value the minute prior to asphyxia (to minimize isoflurane effects) and thus the relative SFI at baseline was 100. One minute prior to asphyxia was chosen as baseline due to post-anesthesia emergence and consequent cerebral hyperemia [20,21]. The median-filtered relative SFI curves were used for further statistical analyses. Relative SFI maps were also created by dividing the baseline SFI from Eq. (3) at each pixel of the SFI map, and a median filter was then applied to images taken over a 10s interval.

We evaluated several CBF characteristics post-ROSC using LSI data. For LSI, these included percent SFI above baseline at hyperemic peak, time from ROSC to hyperemic peak, percent SFI below baseline at the onset of stabilized hypoperfusion, and time from ROSC to the onset of stabilized hypoperfusion. Stabilized hypoperfusion was defined as the initial time when the relative SFI had less than a ± 1% change for at least one min post-ROSC. For each CBF characteristics, we compared the 5- and 7-min asphyxial groups using a Student's t-test, where $p<0.05$ was considered statistically significant and results displayed as mean ± STD.

To assess the correlation between CBF and MAP, we performed a Spearman correlation test for data collected before stabilized hypoperfusion. To quantify the dysregulation between CBF and MAP, we calculated the median difference between relative SFI and relative MAP before and after stabilized hypoperfusion. The difference before and after stabilized hypoperfusion were compared using a paired t-test, where $p<0.05$ was considered statistically significant and results are displayed as mean ± STD.

Raw EEG data were filtered in the following fashion using custom written MATLAB (Mathworks Inc., Natick, MA) code. Data were detrended to remove DC bias and common averaged reference to reduce noise and artifacts across channels [22]. A finite impulse

Biomedical Optics EXPRESS

response (FIR) notch filter at 60Hz was used to remove electrical noise, followed by a FIR bandpass filter from 1 to 150Hz. Signals were then downsampled to 600Hz to reduce computational cost.

To detect the initial EEG burst, we developed an automated algorithm using custom-written MATLAB code. Peaks above 20μV were detected the minute prior to asphyxia and the mean peak value was calculated. Following resuscitation, when the EEG amplitude exceeded 50% of the mean peak value from baseline in the frontal electrodes, a burst was detected. To identify the presence of the initial EEG burst and minimize the effect of noise artifacts, we applied a selection criterion that bursting for five consecutive minutes was necessary. Once bursting occurred for this period, the algorithm reported the initial EEG burst time relative to ROSC, which was used in subsequent analysis. We compared the time from ROSC to initial EEG burst for 5- and 7-min asphyxial groups using a Student's t-test, where $p<0.05$ was considered statistically significant and results are displayed as mean ± STD.

To quantify the total amount of brain perfusion from ROSC to the initial EEG burst, we integrated over time the relative SFI time-course signal from ROSC to initial EEG burst. We used a Spearman correlation test to determine the correlation between total brain perfusion and initial EEG burst time. We then compared the total perfusion from ROSC to initial EEG burst for 5- and 7-min asphyxial groups using a Student's t-test, where $p<0.05$ was considered statistically significant and results are displayed as mean ± STD. We performed the same correlation and statistical comparison using MAP time-course data.

To predict when the initial EEG burst occurred, we calculated a predictive burst ratio that utilized the total perfusion from ROSC to initial EEG burst and normalized to the asphyxial duration Eq. (4).

$$predictive\ burst\ ratio = \frac{\int_{ROSC}^{Burst} (relative\ SFI \text{ or } MAP)dt}{asphyxia\ duration} \tag{4}$$

The predictive burst ratio was calculated for each experiment and the median predictive burst ratio obtained from all experiments for relative SFI and MAP, separately. The predictive burst ratios for 5- and 7-min asphyxial groups were compared using a Student's t-test, where $p<0.05$ was considered statistically significant, and results are displayed as mean ± STD. For relative SFI and MAP individually, the median predictive burst ratio was used to predict when the initial EEG burst would occur. To predict the initial EEG burst we created time plots as a function of the predictive burst ratio, which we called the cumulative predictive burst ratio. To determine the cumulative predictive burst ratio, the upper bound of the integral in Eq. (4) was replaced with time, and incremented by each measurement time point. We then optimized the bounds of a linear fit to the cumulative predictive burst ratio. To obtain the optimal bounds of the linear fit, a range of lower and upper bounds were chosen from 0- to 6-min post-ROSC in 0.25min increments. All possible combinations for the linear fit were tested for each experiment. The bound combination that minimized the median predicted burst time error from all experiments was extracted. This analysis determined the bounds of the linear fit would be from 0.25- to 6-min post-ROSC. The slope (m) and y-intercept (b) were obtained from the linear fit. Using Eq. (5), we extrapolated and predicted the initial EEG burst time.

$$predicted\ burst\ time = m \times (median\ predictive\ burst\ ratio) + b \tag{5}$$

To analyze the performance of the model using CBF and MAP, we computed the percent error of the predicted burst time to the actual burst time and compared the 5- and 7-min asphyxial groups. Results are displayed as median (range).

Biomedical Optics EXPRESS

3. Results

3.1 More severe CA results in longer time to stabilized hypoperfusion

To quantify the precise magnitude (relative to baseline) and time of the hyperemic peak and stabilized hypoperfusion, LSI data were used. An example of relative SFI maps from baseline (Fig. 2(A)), CA (Fig. 2(B)), hyperemia (Fig. 2(C)), and stabilized hypoperfusion (Fig. 2(D)) are shown. We quantified each of the four characteristics (Fig. 2(E)) for both 5- and 7-min asphyxial groups and performed a Student's t-test to compare the groups. The percent change in SFI above baseline (Fig. 2(F)) was non-significant between 5-and 7-min asphyxia ($44.13 \pm 11.06\%$ vs $37.11 \pm 28.80\%$, $p = 0.28$). The time from ROSC to hyperemic peak (Fig. 2(G)) trended shorter for 5-min asphyxia than 7-min asphyxia, but the difference was non-significant (5.19 ± 1.10min vs 5.99 ± 1.26min, $p = 0.12$). The percent change in SFI below baseline (Fig. 2(H)) was equivalent for 5- and 7-min asphyxial groups ($44.95 \pm 9.50\%$ vs $42.26 \pm 11.40\%$, $p = 0.33$). The time from ROSC to stabilized hypoperfusion (Fig. 2(I)) was significantly shorter for 5-min asphyxia than 7-min asphyxia (15.60 ± 3.67min vs 23.76 ± 5.12min, $p = 0.003$).

3.2 CBF and MAP are coupled before stabilized hypoperfusion and uncoupled after stabilized hypoperfusion

To investigate the coupling between CBF and MAP, we examined differences between the relative SFI and MAP time courses (Fig. 3(A)). Both relative SFI and MAP had a sharp decrease as the asphyxial period began (t = 5min), and each had an overshoot phase post-ROSC (t ~15min). After the hyperemic phase, the relative SFI time-course was at a large deficit compared to baseline (~70% below baseline), while the MAP returned to near baseline (~100mmHg). To quantify the similarities, we used a Spearman correlation test before stabilized hypoperfusion (Fig. 3(B)). Our results show that MAP and CBF are highly correlated before stabilized hypoperfusion for each experiment, with highly statistically significant correlation coefficients ($R = 0.75 \pm 0.1$, $p < 1.4 \times 10^{-92}$). To quantify the dysregulation between CBF and MAP, we calculated the median difference between relative SFI and relative MAP before and after stabilized hypoperfusion. The median difference between relative SFI and relative MAP before stabilized hypoperfusion was significantly higher (CBF and MAP are more close) than after stabilized hypoperfusion (-16.67 ± 9.13 vs -68.06 ± 11.72, $p = 1.5 \times 10^{-8}$). Of note, there was no significant difference between the correlation coefficients of 5- and 7-min asphyxia durations (0.77 ± 0.12 vs 0.73 ± 0.08, $p = 0.59$).

3.3 Initial EEG burst begins after CBF hyperemic phase and before stabilized hypoperfusion

To investigate the relationship between restarting brain electrical activity to CBF after resuscitation, we studied the timing of the initial EEG burst with respect to the CBF time-course. First, we determined when the initial EEG burst occurred for 5- and 7-min asphyxial durations (Fig. 4(A)). We compared the performance of our automated detection algorithm to visual detection of the initial EEG burst. The mean percent error was less than 1% for all experiments. The time from ROSC to initial EEG burst (Fig. 4(B)) was significantly shorter for 5-min asphyxia than 7-min asphyxia (12.17 ± 2.17min vs 16.97 ± 3.67min, $p = 0.007$).

Biomedical Optics EXPRESS

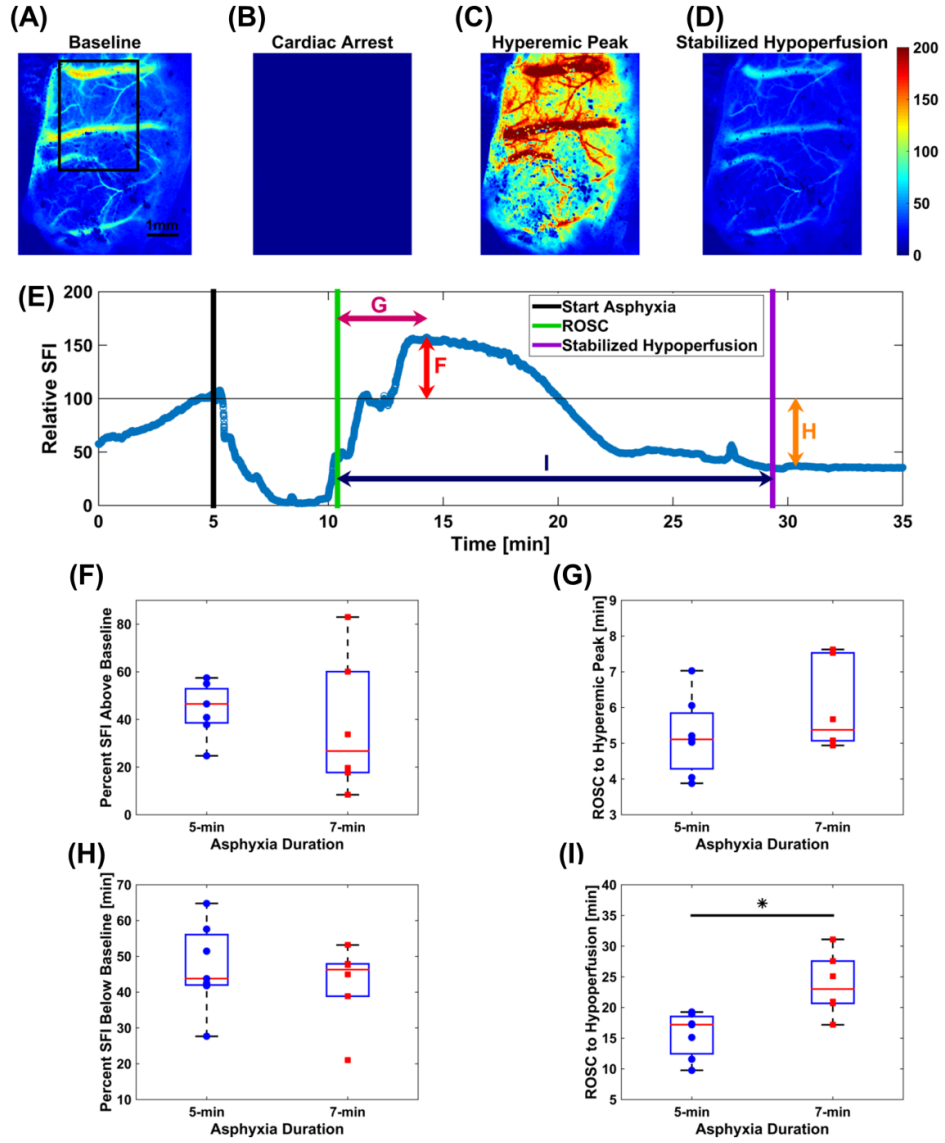

Fig. 2. CBF characteristics. Median-filtered relative SFI maps from a representative 5-min asphyxia experiment acquired during (A) baseline, where black rectangle represents ROI selected to avoid specular reflection, and a 1mm scale bar, (B) cardiac arrest, (C) hyperemic peak, and (D) stabilized hypoperfusion. The vertical color bar indicates relative SFI units. (E) A representative 5-min asphyxia experiment that shows relative SFI time course plot with schematic of CBF characteristics. Black vertical line represents start of asphyxia, green vertical line represents ROSC, and purple vertical line represents stabilized hypoperfusion. Double-arrowed red line with letter F represents percent SFI above baseline at hyperemic peak, double-arrowed dark magenta line with letter G represents time from ROSC to hyperemic peak, double-arrowed orange line with letter H represents percent SFI below baseline at stabilized hypoperfusion, double-arrowed navy blue line with letter I represents time from ROSC to stabilized hypoperfusion. Comparison between 5- and 7-min asphyxial durations for (F) percent SFI above baseline at hyperemic peak ($44.13 \pm 11.06\%$ vs $37.11 \pm 28.80\%$, $p = 0.28$), (G) time from ROSC to hyperemic peak (5.19 ± 1.10min vs 5.99 ± 1.26min, $p = 0.12$), (H) percent SFI below baseline at stabilized hypoperfusion ($44.95 \pm 9.50\%$ vs $42.26 \pm 11.40\%$, $p = 0.33$), (I) time from ROSC to stabilized hypoperfusion (15.60 ± 3.67min vs 23.76 ± 5.12min, $p = 0.003$). Asterisk represents significant differences ($p < 0.05$).

Biomedical Optics EXPRESS

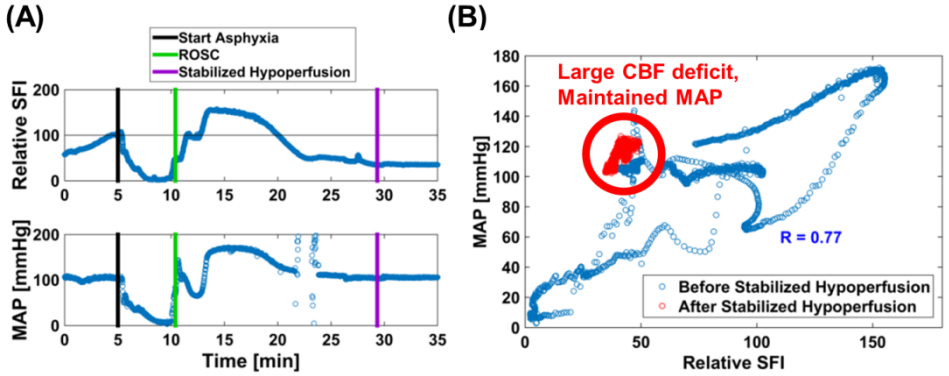

Fig. 3. CBF and MAP comparison. (A) A representative 5-min asphyxia experiment that shows relative SFI (top) and MAP (bottom) time-course plots. Black vertical line represents start of asphyxia, green vertical line represents ROSC, and purple vertical line represents stabilized hypoperfusion. The relative SFI time-course shows that CBF is much lower than baseline at stabilized hypoperfusion, while the MAP is nearly 100mmHg at stabilized hypoperfusion. The gap from ~21- to 23-min on the MAP time-course is due to ABG being taken. (B) The same 5-min asphyxia experiment from (A) that compares MAP and relative SFI before stabilized hypoperfusion (blue) and after stabilized hypoperfusion (red). Before stabilized hypoperfusion MAP and relative SFI are significantly correlated for the representative rat ($R = 0.77$, $p = 1 \times 10^{-93}$). After stabilized hypoperfusion, CBF is at a major deficit compared to baseline, while MAP is maintained near baseline, circled in red.

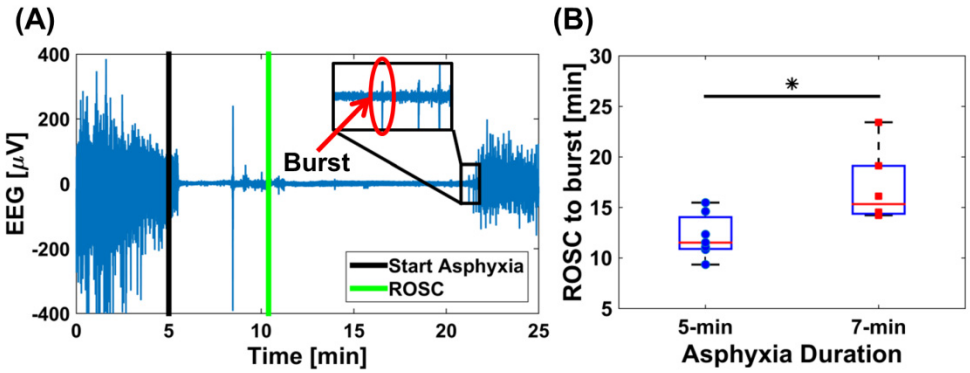

Fig. 4. Initial EEG burst. (A) A representative 5-min asphyxia experiment that shows EEG time-course to illustrate detection of initial EEG burst post-ROSC. EEG data shown was recorded from the upper-left electrode in Fig. 1(C). Black vertical line represents start of asphyxia, green vertical line represents ROSC, and red circle of inset is the first EEG burst detected by automated algorithm post-ROSC. (B) Comparison between 5-min and 7-min asphyxial durations for the time from ROSC to initial EEG burst (12.17 ± 2.17min vs 16.97 ± 3.67min, $p = 0.007$). Asterisk represents significant difference ($p < 0.05$).

We observed the initial EEG burst always occurred as CBF decreased toward stabilized hypoperfusion (Fig. 5(A)), which led to the hypothesis that a threshold amount of CBF is necessary to restart brain electrical activity following resuscitation from CA. We quantified total brain perfusion from ROSC to initial EEG burst as the time-integrated relative SFI. We also performed this analysis with MAP, as our previous results show MAP and relative SFI are correlated before stabilized hypoperfusion (Fig. 3(B)). Using the Spearman correlation test, our results show a significant positive correlation between time-integrated relative SFI and time to initial EEG burst ($R = 0.84$, $p = 0.0003$; Fig. 5(B)). Similarly, our results show a significant positive correlation between time-integrated MAP and time to initial EEG burst ($R = 0.80$, $p = 0.001$; Fig. 5(C)).

Biomedical Optics EXPRESS

We then compared 5- and 7-min asphyxial groups. Our results show that significantly less time-integrated relative SFI (1290 ± 140 vs 1781 ± 286, p = 0.002) and non-significantly less time-integrated MAP (1331 ± 257 vs 1645 ± 378, p = 0.1) is necessary to initiate EEG bursting for 5-min asphyxia than 7-min asphyxia (Fig. 5(D) and 5(E), respectively). These results indicate there is not a threshold of CBF to restart brain electrical activity following resuscitation from different severities of asphyxial CA, and thus our initial hypothesis was incorrect. Therefore, based on these results, we normalized the time-integrated relative SFI and MAP to the asphyxial duration to create an asphyxial invariant threshold; we call this term the predictive burst ratio (Eq. (4). The predictive burst ratio had less spread using CBF (256 ± 33) than MAP (252 ± 53). The predictive burst ratio was not significantly different between 5- and 7-min asphyxial durations (Fig. 5(F) and 5(G), respectively) for relative SFI (258.0 ± 28.1 vs 254.5 ± 40.8, p = 0.86) and MAP (269.7 ± 47.5 vs 249.7 ± 43.3, p = 0.45). These calculations suggest that normalizing the total perfusion to the asphyxial duration is an appropriate normalization term.

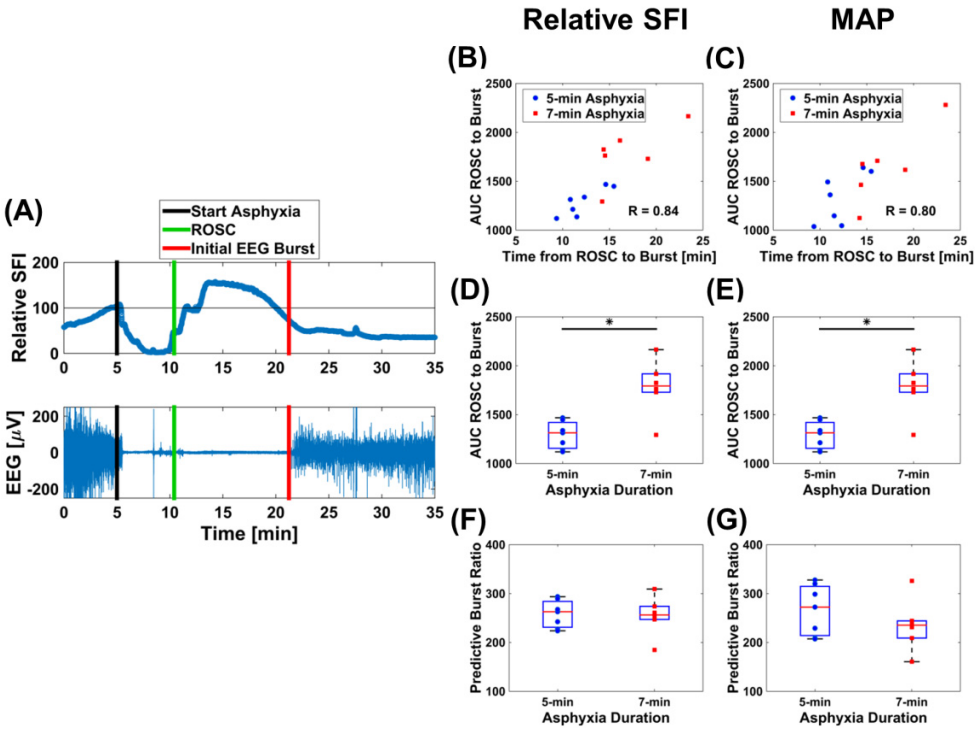

Fig. 5. Initial EEG burst begins after CBF hyperemic phase and before stabilized hypoperfusion. (A) Representative relative SFI and EEG time-courses to illustrate initial EEG burst occurs after CBF hyperemic phase and before stabilized hypoperfusion. EEG data shown was recorded from the upper-left electrode in Fig. 1(C). Black vertical line represents start of asphyxia, green vertical line represents ROSC, and red vertical line represents initial EEG burst. (B and C) AUC from ROSC to burst vs time to burst after ROSC shows a significant positive correlation for relative SFI (left) (R = 0.84, p = 0. 0003) and MAP (right) (R = 0.80, p = 0. 001). (D and E) AUC from ROSC to burst is significantly less for 5-min asphyxia than 7-min asphyxia for relative SFI (left) (1290 ± 140 vs 1781 ± 286, p = 0.002) and non-significantly time-integrated MAP (right) (1331 ± 257 vs 1645 ± 378, p = 0.1). (F and G) The predictive burst ratio was non-significant comparing 5- and 7-min asphyxial durations for relative SFI (left) (258.0 ± 28.1 vs 254.5 ± 40.8, p = 0.86) and MAP (right) (269.7 ± 47.5 vs 249.7 ± 43.3, p = 0.45). Asterisks represent significant differences (p <0.05).

Biomedical Optics EXPRESS

3.4 CBF predicts initial EEG burst for 5-min asphyxia, but is a poor predictor for 7-min asphyxia

To assess the accuracy of the predictive burst ratio, we performed linear regression to the cumulative predictive burst ratio from 0.25- to 6-min post-ROSC and extrapolated the linear fit using the median predictive burst ratio to predict the initial EEG burst time (Eq. (5). Examples of the predictive model using CBF and MAP for 5- and 7-min asphyxia are shown in Fig. 6. The median percent error for relative SFI and MAP were 8.21% (range = 1.57% – 80.97%) and 12.10% (range = 3.39% – 133.92%), respectively. Since the percent error range of predicting the initial EEG burst was large, we assessed how 5- and 7-min asphyxial groups compared. The 5-min asphyxial group was associated with a considerably lower median percent error than the 7-min asphyxial group for relative SFI [3.46% (range = 1.57% – 17.22%) vs 31.22% (range = 7.95% – 80.97%)] and for MAP [8.01% (range = 3.39% – 23.40%) vs 40.80% (range = 9.34% – 133.92%)], respectively. These results suggest that CBF and MAP more accurately predict onset of EEG bursting for 5-min asphyxia than for 7-min asphyxia, and that CBF predicts better than MAP for both 5- and 7-min asphyxial durations.

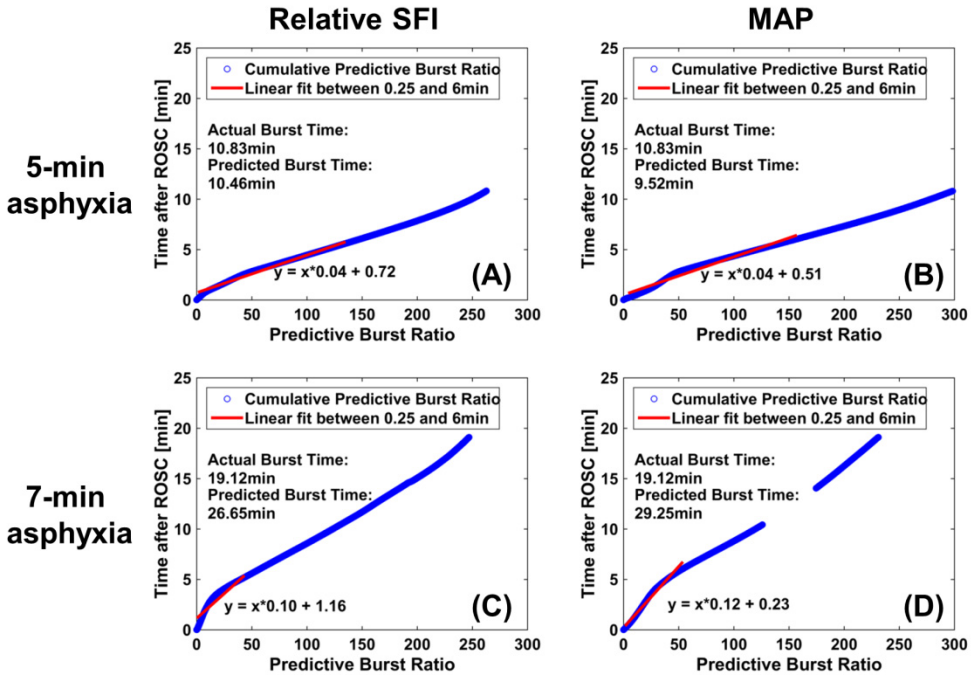

Fig. 6. Representative predictive burst times for initial EEG burst using predictive burst model. (A) A representative 5-min asphyxial experiment that used relative SFI data to predict the initial EEG burst time, percent error of 3.42% obtained. (B) Same 5-min asphyxial experiment used as (A), but used MAP to predict initial EEG burst time, percent error of 12.10% obtained. (C) A representative 7-min asphyxial experiment that used relative SFI to predict initial EEG burst time, a percent error of 39.37% obtained. (D) Same 7-min asphyxial experiment used as (C), but used MAP to predict initial EEG burst time, percent error of 52.96% obtained. Gap from ~140 to ~170 of predictive burst ratio is due to ABG being taken.

4. Discussion and conclusion

Using a multi-modal platform, we demonstrate a number of novel findings elucidating the relationship between brain electrical activity and hemodynamics during CA and resuscitation. Our platform combined LSI, arterial blood pressure, and EEG to quantitatively assess CBF, MAP, and brain electrophysiology dynamics during CA and resuscitation.

Biomedical Optics EXPRESS

CBF is known to have distinct phases following resuscitation from CA [15]. In this study we quantified the precise magnitude (relative to baseline) and time of the hyperemic peak and stabilized hypoperfusion post-ROSC (Fig. 2(E)-2(I)), due to our system's relatively high temporal resolution (~seconds). Previous studies have not been able to identify the exact time and magnitude of the hyperemic peak and stabilized hypoperfusion post-ROSC due to the relatively poor temporal resolution (~5–30min) [7,10,23]. Interestingly, in a pediatric model of asphyxial CA, Manole et al. [9] and Shaik et al. [24] both did not observe a hyperemic peak in cortical CBF using MRI and LSI, respectively. Their results suggest that post-ROSC cerebral hemodynamics vary between adults and children. These varying dynamics, may suggest the need to treat adults and children differently following resuscitation from asphyxial CA.

Under normal conditions, the brain is highly regulated as CBF is constant over a wide range of MAP. Previous studies have examined cerebrovascular autoregulation following CA. These studies have generally reported that the lower limit of autoregulation increases post-ROSC [5]. Our results are in line with these findings, as MAP returned to near baseline post-ROSC, while CBF was at a major deficit after the onset of stabilized hypoperfusion (Fig. 3(B)). Furthermore, to assess which asphyxial duration had more cerebrovascular dysregulation, we compared the median difference between relative SFI and relative MAP for 5- and 7-min asphyxial durations after stabilized hypoperfusion. We observed a trend towards CBF more closely resembling MAP for 7-min than 5-min asphyxial duration (-62.70 ± 14.58 vs -72.65 ± 6.67, $p = 0.13$). This may possibly suggest that more severe CA is associated with increased cerebrovascular dysregulation (i.e. CBF more closely resembles MAP), though future studies with higher sample size may be needed to conclude this definitely. Since MAP is a parameter clinicians depend on to indirectly monitor cerebral perfusion post-ROSC, our results suggest that direct CBF measurement may be necessary to adequately assess and optimize cerebral perfusion for different severities of CA.

Many studies have investigated the evolution of brain electrical activity post-ROSC [25,26], while few have reported the time point at which EEG activity resumes post-ROSC [11,27]. To our knowledge, only one study analyzed the onset of EEG bursting with relation to neurological outcome. Chen et al. showed a faster onset of EEG bursting in hypothermia-treated rats, which also had better neurological outcome at 96h post-ROSC [27]. Our results show that more severe CA, which results in worse neurological outcome [12], resulted in longer time to initial EEG burst (Fig. 4(B)). However, the mechanism that drives the brain to restart following resuscitation is not well understood. Our data suggests that CBF is a key component of this mechanism.

We observed that the initial EEG burst occurred after the hyperemic peak, but prior to stabilized hypoperfusion (Fig. 5(A)). We then investigated whether a threshold of CBF is necessary to restart brain electrical activity. Our results suggest that more perfusion is necessary to restart brain electrical activity for 1) a longer time to initial EEG burst (Fig. 5(B)) and 2) more severe CA (Fig. 5(D)). Due to this, we normalized the total perfusion by the asphyxial duration to develop an empirical predictive burst ratio (Fig. 5(F)). We plan to use the median predictive burst ratio from these experiments to predict when the initial EEG burst occurs in future experiments. In the present study, the median predictive burst ratio, and predictive model were able to predict the initial EEG burst well for 5-min asphyxia (3.46% error) (Fig. 6(A)), but poorly for 7-min asphyxia (31.22% error) (Fig. 6(C)). These results suggest that a threshold of cerebral reperfusion is both necessary and sufficient to restart brain electrical activity following 5-min asphyxia, but this condition alone is not sufficient for brain electrical activity to resume following 7-min asphyxia. We hypothesize that the large burst prediction error for 7-min asphyxia is due to increased cerebral metabolic deficiency, cerebrovascular dysregulation, and an imperfect linear fitting method during the initial minutes post-ROSC. To test our hypothesis, future studies will be focused on developing a revised empirical predictive model that utilizes the cerebral metabolic rate of oxygen to

Biomedical Optics EXPRESS

describe the initial EEG burst [28–30]. In short, knowledge of when EEG activity will recover may potentially equip clinicians with more accurate prognostication, better treatments for post-CA coma, and improve neurological outcome.

Limitations exist in our study. Despite the statistically significant results and trends identified in this study, the power of these findings is limited due to a small sample size. In addition, these experiments used a full craniectomy, which may change the intracranial pressure. In the future we plan to perform experiments with a thinned-skull cranial window to minimize this effect.

In conclusion, we have developed a multi-modal approach to quantify CBF, MAP, and brain electrophysiology dynamics with high temporal resolution, in an asphyxial CA model. Our multi-modal approach combines LSI, arterial blood pressure, and EEG into a preclinical monitoring setup that effectively mimics an intensive care unit. Our results quantify the time and magnitude of the hyperemic peak and stabilized hypoperfusion post-ROSC. Furthermore, we show that CBF and MAP are well correlated before stabilized hypoperfusion, but CBF is at a large deficit after stabilized hypoperfusion, despite normal MAP. Finally, we demonstrate that EEG bursting begins after the CBF hyperemic phase and before stabilized hypoperfusion, and we can predict when the initial EEG burst occurs for less severe CA well. Together, these results indicate the importance of using multi-modal approaches to investigate CA recovery to better understand physiological processes and ultimately allow for novel therapeutic approaches that improve neurological outcome.

Funding

We gratefully acknowledge support from the Arnold and Mabel Beckman Foundation, the United States National Institutes of Health (grant number P41EB015890), the National Science Foundation Graduate Research Fellowship Program under Grant No. DGE-1321846 to Christian Crouzet, the Hewitt Foundation for Medical Research and ICTS 1TL1TR001415-01 to Dr. Robert H. Wilson, and KL2 grant via NIH CTSA UL1 TR001414 and funds from the Department of Neurology, School of Medicine to Dr. Yama Akbari.

Acknowledgments

We would like to thank the Beckman Laser Institute Microvascular Therapeutics and Imaging lab and Akbari lab for their support and input in this work.